Research Article | Vol. 25, No. 23 | 13 Nov 2017 | OPTICS EXPRESS 28442
Optics EXPRESS

Bragg gratings inscribed in selectively inflated photonic crystal fibers

CHAO WANG,[1,2] JUN HE,[1] JINGCHUAN ZHANG,[3] CHANGRUI LIAO,[1] YING WANG,[1] WEI JIN,[4] YIPING WANG,[1,5] JUNHUA WANG[2,6]

[1]*Key Laboratory of Optoelectronic Devices and Systems of Ministry of Education and Guangdong Province, College of Optoelectronic Engineering, Shenzhen University, Shenzhen 518060, China*
[2]*School of Electrical Engineering, Wuhan University, Wuhan, 430072, China*
[3]*Beijing Institute of Spacecraft Environment Engineering, Beijing, 100094, China*
[4]*Department of Electrical Engineering, the Hong Kong Polytechnic University, Hung Hom, Hong Kong, China*
[5]*ypwang@szu.edu.cn*
[6]*junhuawang@whu.edu.cn*

Abstract: We report a method for effective fabrication of Bragg gratings in all-silica photonic crystal fibers (PCF). The problem of cladding-hole scattering in PCF grating inscription is avoided by selectively inflating a section of PCF, resulting a locally suspended-core fiber (SCF) region with relatively simple cladding structure. Hence, the inscription laser can laterally access to the core region with little loss. In the SCF regions with core diameter ranging from 2 to 4.5 μm, first-order Bragg gratings are fabricated by use of a phase mask and a focused infrared femtosecond laser with pulse energy as low as ~200 μJ. For the same grating period, samples with different core sizes exhibit different resonant wavelengths and spectral properties, which would enable a range of applications in grating-integrated PCF sensors and devices.

OCIS codes: (060.3735) Fiber Bragg gratings; (060.2340) Fiber optics components; (060.2370) Fiber optics sensors; (060.5295) Photonic crystal fibers; (060.4005) Microstructured fibers.

References and links

1. G. D. Marshall, R. J. Williams, N. Jovanovic, M. J. Steel, and M. J. Withford, "Point-by-point written fiber-Bragg gratings and their application in complex grating designs," Opt. Express **18**(19), 19844–19859 (2010).
2. A. D. Kersey, M. A. Davis, H. J. Patrick, M. LeBlanc, K. Koo, C. Askins, M. Putnam, and E. J. Friebele, "Fiber grating sensors," Lightwave Technology. Journalism **15**, 1442–1463 (1997).
3. F. Berghmans, T. Geernaert, T. Baghdasaryan, and H. Thienpont, "Challenges in the fabrication of fibre Bragg gratings in silica and polymer microstructured optical fibres," Laser Photonics Rev. **8**, 27–52 (2014).
4. L. Fu, G. Marshall, J. Bolger, P. Steinvurzel, E. Mägi, M. Withford, and B. Eggleton, "Femtosecond laser writing Bragg gratings in pure silica photonic crystal fibres," Electron. Lett. **41**, 638–640 (2005).
5. N. Groothoff, I. Canning, E. Buckley, K. Lyttikainen, and J. Zagari, "Bragg gratings in air-silica structured fibers," Opt. Lett. **28**(4), 233–235 (2003).
6. G. D. Marshall, D. J. Kan, A. A. Asatryan, L. C. Botten, and M. J. Withford, "Transverse coupling to the core of a photonic crystal fiber: the photo-inscription of gratings," Opt. Express **15**(12), 7876–7887 (2007).
7. S. J. Mihailov, D. Grobnic, H. Ding, C. W. Smelser, and J. Broeng, "Femtosecond IR laser fabrication of Bragg gratings in photonic crystal fibers and tapers," IEEE Photonics Technol. Lett. **18**, 1837–1839 (2006).
8. H. R. Sørensen, J. Canning, J. Lægsgaard, K. Hansen, and P. Varming, "Liquid filling of photonic crystal fibres for grating writing," Opt. Commun. **270**, 207–210 (2007).
9. M. Konstantaki, P. Childs, M. Sozzi, and S. Pissadakis, "Relief Bragg reflectors inscribed on the capillary walls of solid-core photonic crystal fibers," Laser Photonics Rev. **7**, 439–443 (2013).
10. C. Wang, W. Jin, W. Jin, J. Ju, J. Ma, and H. L. Ho, "Evanescent-field photonic microcells and their applications in sensing," Measurement **79**, 172–181 (2016).
11. N. N. David, "Multi-photon high-excitation-energy approach to fibre grating inscription," Meas. Sci. Technol. **18**, R1 (2007).
12. C. Wang, W. Jin, C. Liao, J. Ma, W. Jin, F. Yang, H. L. Ho, and Y. Wang, "Highly birefringent suspended-core photonic microcells for refractive-index sensing," Appl. Phys. Lett. **105**, 061105 (2014).
13. J.-L. Kou, M. Ding, J. Feng, Y.-Q. Lu, F. Xu, and G. Brambilla, "Microfiber-based Bragg gratings for sensing applications: a review," Sensors (Basel) **12**(7), 8861–8876 (2012).
14. S. J. Mihailov, D. Grobnic, C. W. Smelser, P. Lu, R. B. Walker, and H. Ding, "Bragg grating inscription in various optical fibers with femtosecond infrared lasers and a phase mask," Opt. Mater. Express **1**, 754–765 (2011).
15. C. Wang, W. Jin, J. Ma, Y. Wang, H. L. Ho, and X. Shi, "Suspended core photonic microcells for sensing and device applications," Opt. Lett. **38**(11), 1881–1883 (2013).

#307600 https://doi.org/10.1364/OE.25.028442
Journal © 2017 Received 22 Sep 2017; revised 23 Oct 2017; accepted 25 Oct 2017; published 1 Nov 2017

Optics EXPRESS

1. Introduction

The widely-used fiber Bragg gratings (FBGs) have been realized on various optical fibers by using high power lasers and interferometric or point-by-point inscription methods [1,2]. However, for the new generation fibers with complicate cladding structures, such as the photonic crystal fibers (PCFs), two major challenges existed in applying conventional grating inscription methods: the large cladding scattering and distortion to transvers incident laser beam, and the low photosensitivity of fiber material due to the lack of necessity of the doping process for optical wave guidance [3].

High power ultraviolet (UV) and femtosecond (fs) radiation have been successfully applied on fabricating Bragg gratings in the pure silica PCFs [4, 5]. Nevertheless, the challenges of cladding scattering and distortion still hamper the efficiency in building high quality PCF gratings in the terms of long exposure time, high inscription power and low grating reflectivity. Many techniques have been proposed to alleviate the scattering problem: The hydrogen-loading would be helpful to enhance the laser-induced refractive index (RI) changing in pure silica PCF [4], although the hydrogen out-diffusion problem for the holey fibers might weaken the effect of enhancement. Optimizing the lateral incident angle of inscription laser would improve the transfer of laser power to the core region by the factor of ~2 [6]. In addition, several fiber post-processing techniques, such as the tapering [7] and liquid or absorber layer assistant inscription [8, 9], would facilitate the grating inscription in PCFs, but might introduce several additional problems, such as large optical loss, poor spectral quality and material residuals in fiber.

Here we report a new method for FBG inscription in commercial all-silica PCFs. The scattering and distortion problems are avoid by locally transferred the PCF to a section of suspended-core fiber (SCF), as shown in Fig. 1. The SCF region possesses a simpler cladding structure including just few hole-columns and a thin jacket tube, and connects to the un-processed PCF regions at its both ends via low-loss transitions. By use of a near-infrared fs laser and a phase mask, Bragg gratings have been fabricated in the SCF regions with low pulse energy and short exposure time. Basic characteristics of the grating embedded PCFs were simulated and experimentally investigated.

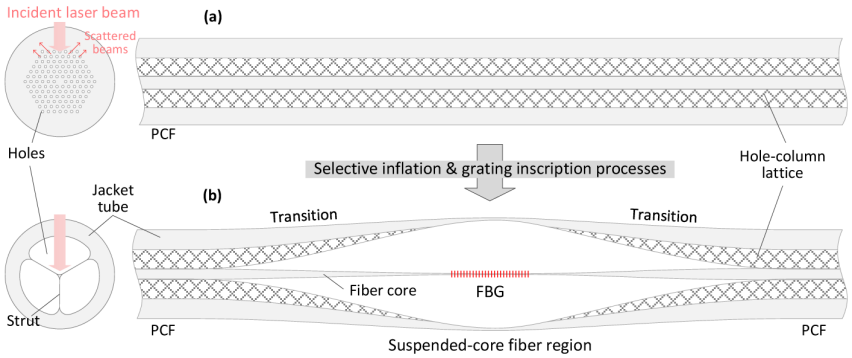

Fig. 1. Schematics of cross-sectional structures of (a) a PCF and (b) a selectively inflated PCF for Bragg grating inscription. The left and right figures are respectively the cross-sections perpendicular to and along the fiber axis.

2. Grating inscription

Our grating inscription process involves two major steps: the selectively inflation of a PCF and grating inscription in the processed region. The commercial available PCF, ESM-12 from NKT Photonics, was used in our experiments.

2.1. Selective inflation of PCF

The selectively inflation technique has been reported in [10] and is versatile in fabricating various local SCF structures along a PCF. In the fabrication, the combination effect of the collapsing and expansion of different hole-columns in a PCF eventually forms a region with SCF structure, which have a micro-/nano-sized core supported inside the fiber by

Optics EXPRESS

several struts and connected at its both sides to the unprocessed PCF regions via low-loss transitions (typically <0.1 dB).

Among all the possible SCF structures given in [10], the three-hole SCF structure was chosen for grating inscription for the least internal components which would be helpful to minimize the possible scattering and distorting of the grating inscription beam. Figure 2(a) is the cross-sectional image of a three-hole SCF sample produced the by the selective inflation process. The sample possesses a triangular-like core with inscribed circle diameter of ~4.5 μm and three struts with width of ~400 nm. The core diameter of the sample can be tailored in the range from ~4.8 μm to ~700 nm by controlling the distance and speed of axial stretch in fabrication. The red arrow in Fig. 2(a) indicates an optimal direction for grating inscription, at which the influence from struts would be minimum. Figure 2(b) is the image of a sample taken from the optimal direction. The fiber core region can be clearly observed and is far from the shadow of struts (the thick black lines). However, the processed region typically exhibits a spindle-like shape due to the larger degree of expansion in the central heat region during the fabrication. The curved surface might disturbs of side-incident beam and cause unwanted chirp effect in grating spectrum. To solve the problem, we released the internal gas pressure of the sample with curved surface, then heated and axially elongated the SCF region again by using a fiber-tapering machine. As shown in Fig. 2(c), the SCF region exhibits a flatten surface after the process.

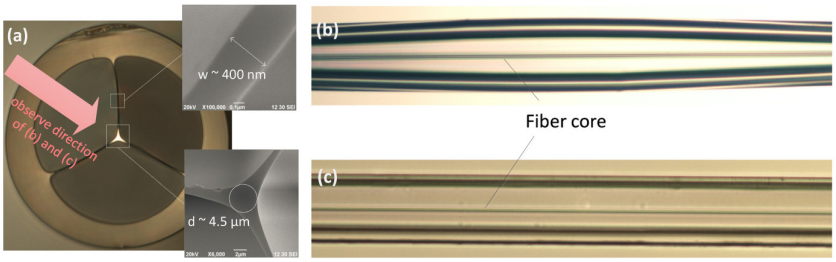

Fig. 2. (a) Cross-sectional micrographs of a three-hole SCF sample made by the selective inflation technique. Side-view micrograph of a SCF region (b) before and (c) after an additional flattening process.

2.2. Bragg grating Inscription

The grating inscription system as Fig. 3(a) was used in our fabrication. The beam of a Ti:sapphire fs laser (800 nm, 100 fs, 1 kHz, Spectra-Physics) is focused by a cylindrical lens with focal length of 50 mm. A phase mask (Ibsen Photonics) with period of 1.07 μm is placed behind the cylindrical lens and ~300 μm to the focus of lens. The $1/e^2$ Gaussian diameter of the fs laser beam is ~6.2 mm. The focal width and Rayleigh length of the cylindrical lens are, respectively, calculated to be 8.3 μm and 66.8 μm. The focal region for grating inscription is small but enough to cover the fiber core. A CCD camera is adopted in Fig. 3(a) to assist the core positioning and adjusting the azimuth angle of SCF region. When the fiber core and focal region is in good alignment, white light can be observed on the fiber core.

Since the Rayleigh length of the focused fs laser is much larger than the core size, a section of strut in the SCF region would be involved in the inscription region during the inscription, resulting the formation of slight scratches as the inset of Fig. 3(b) on the thin strut and close to the fiber core. In the fabrication, a long-focus lens could facilitate the core positioning, however would bring the risk of damaging the delicate in-fiber structure due to the large inscription region and the demand to high pulse energy of fs laser. The damage of the delicate in-fiber structure would generate a large amount of debris as Fig. 3(c) and increase the loss of sample significantly.

Optics EXPRESS

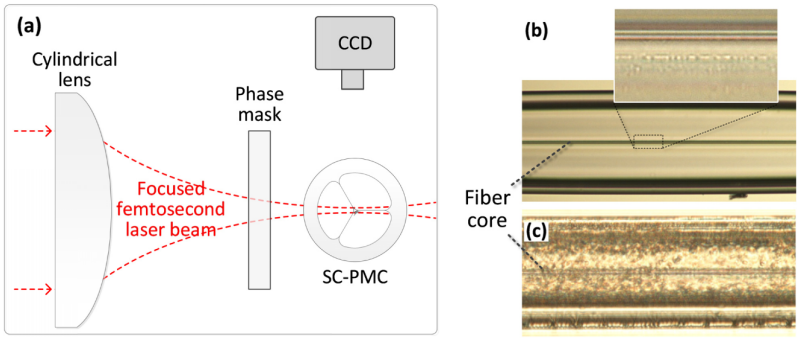

Fig. 3. (a) Schematic of the experiment setup for FBGs inscription in the three-hole SCF region. Images of grating samples inscribed by use of cylindrical lens with focus length of (b) 50 mm and (c) 120 mm respectively.

Figure 4(a) shows the transmission and reflection spectra of a grating inscribed in the SCF region with core diameter of ~3.3 μm. In the fabrication, the pulse energy started from ~200 μJ (peak intensity of ~7.5×10^{12} W/cm^2). The transmission and reflection spectra were recorded by using a wideband light source (Amonics ALS-CWDM-FA) and an optical spectrum analyzer (OSA, Yokogawa AQ6370C). When the fiber core was exposed to the focused fs laser, a grating reflection peak appeared quickly at the wavelength of ~1516.05 nm. The transmission dip increased to ~2 dB in ~5 seconds. However, the grating spectra stayed as the light gray line in Fig. 4 with even longer exposure. The index modulation of the grating is calculated to be ~5.7×10^{-5}. Then, the pulse energy was increased to 240 μJ. The grating continued to increase to ~9 dB in ~300 seconds and stopped again. In the second process, the index modulation increased to ~1.4×10^{-4} and the loss increased from 0.08 dB to 0.24 dB; The grating wavelength experienced a blue shift of 0.29 nm, which might indicate a negative index change induced by the multi-photon process and the formation of a type-II grating [11]. Figure 3(b) is the side-view image of the sample's grating region. In the strut located in the focal region of inscription beams, scratches can be observed. Since the scratches are far from (~4 μm) the core region and poor in periodicity, the structural and index modulations should be formed in most of the core region, however can hardly observed with optical microscope. Influence of the scratches will be discussed in the next section with simulation.

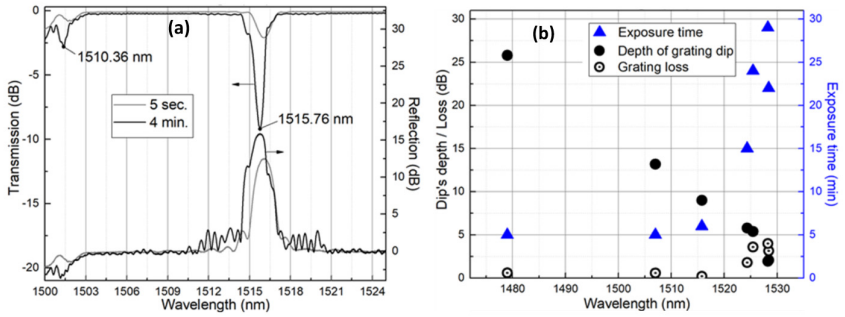

Fig. 4. (a) Spectra of Bragg grating built in a SCF region with core diameter of ~3.3 μm. (b) The grating depth, loss and exposure time of grating samples with different resonant wavelengths.

A peak of polarization dependent loss of the sample was measured to be ~2.8 dB at the short wavelength edge of the grating dip by use of a photonic all-parameter analyzer (Agilent 81910A). The 3dB-bandwidth of the grating is ~1 nm which could be narrowed down by increasing grating length through expanding the fs laser beam diameter or using scanning focus techniques. The small dip at 1501.36 nm in the transmission spectrum reveals a coupling from the fundamental mode to a lossy higher order mode, which might be caused by the tilt of the grating structure.

Optics EXPRESS

By using the inscription method, more Bragg gratings were inscribed in SCF regions with different core diameters ranging from 2 μm to 4.5 μm. The same phase mask was used in the fabrication. The sample with a smaller core size would exhibited a shorter resonant wavelength. The relationship between core size and Bragg wavelength will be discussed in the next section. Figure 4(b) shows the grating depth, losses and exposure time of the samples built with the same pulse energy of ~240 μJ. For the samples with shorter Bragg wavelength (i.e. smaller core sizes), the grating resonances were found to be stronger and the exposure time is shorter. This could be explained by the stronger index modulation would be produced by the fs laser induced structural changes in the SCF region with smaller core. Figure 5(a) shows the spectra of a 25 dB-depth grating fabricated with exposure time of ~5 minutes on the SCF region with core diameter of ~2 μm. In comparison, Fig. 5(b) shows the grating sample with core diameter of ~4.5 μm. The grating depth is just ~2 dB for more than 25 minutes exposure time. The longer exposure time for the samples with larger core size might be the reason of larger loss. The additional spectrum (upper red line) in Fig. 5(b) is the reflection spectrum with ~4% reflection from the flat fiber-end connected to the sample. The spectrum was used as a reference to estimate the grating reflectivity at the beginning of the fabrication when the grating reflection is weak.

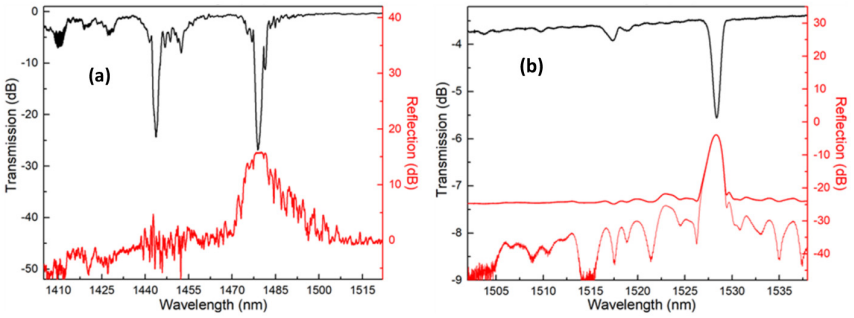

Fig. 5. The transmission and reflection spectra of two FBG samples fabricated in SCF region with core diameter of (a) 2 μm and (b) 4.5 μm respectively.

3. Model and simulation

To understand the properties of the grating in the three-hole SCF regions, we built a model as Fig. 6(a) for the triangular-like fiber core, and simulated the SCFs with different core sizes and ambient RIs (n_a) adjacent to the core by using the finite element method (FEM) software COMSOL. The core is represented by the dark region enclosed by three arc curves with radius $\boldsymbol{R = (3/2 + \sqrt{3})d-(2 + \sqrt{3})s}$, where $\boldsymbol{d}$ is the dimeter of the inscribed circle of the core region, $\boldsymbol{s}$ is the width of strut. According to the SEM images of samples, the ratio d/s could be simplified to a constant of 11.5 for SCF regions with core diameter ranging from 2 to 4.5 μm, hence R≈2.9d.

Figure 6(b) and (c) demonstrate the calculated energy profiles and electrical field vectors of (b) the fundamental mode and (c) a first group higher order mode for a 3.3-μm-diameter SCF model at the wavelength of 1550 nm. The higher order modes would be cut-off when the core diameter is smaller than 700 nm. In model of Fig. 6(d), part of a strut is removed to simulate the scratch region as shown in the inset of Fig. 3(b). The cut point is 4 μm to the center of core. The calculated effective index of the fundamental mode is ~8×10^{-7} lower than fundamental mode of the original core structure. This might indicates the scratches in the strut contribute little to the index modulation of the grating (10^{-4} level). However, for the SCF regions with core sizes in sub-wavelength scale, the grating spectra could be strongly affected by the structure damage near the core region.

Optics EXPRESS

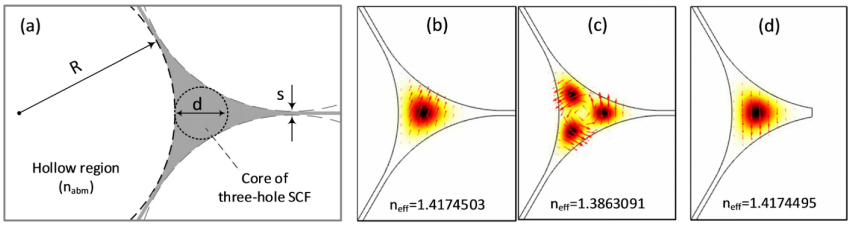

Fig. 6. (a) Model of the core region of a three-hole SC-PMC. (b-d) Simulated energy profile and electrical field distribution of (b) the fundamental mode, (c) a first group higher order mode, and (d) the fundamental mode of the core region with two struts.

The SCF regions with adiabatic transitions were used in our grating fabrication for the reason of low loss and mode interference. In these SCF regions, the transmission light mainly propagates in fundamental mode and exhibits a smooth spectrum. Under the perturbation of the Bragg grating structure, the fundamental mode can be coupled to the backward fundamental mode, as well as the lossy higher order modes, which would cause a multi-dip spectrum in transmission. The coupling wavelengths of the fundamental mode in various SCF regions can be estimated by using the equation $m \cdot \lambda = (n_{eff,0} - n_{eff,res}) \cdot \Lambda$, where m is the order of grating resonance. λ is the operation wavelength. Λ is the grating pitch which is 535 nm in our experiment. $n_{eff,0}$ and $n_{eff,res}$ are respectively the effective RI of the fundamental mode and a target mode to the coupled. For the first order coupling between the forward and backward fundamental mode, the formula can be simplified as: $\lambda = \lambda_B = 2n_{eff,0} \cdot \Lambda$. The SCFs with smaller core exhibit low modal effective RIs, resulting the blue shift of the Bragg resonant wavelength. In Fig. 7(a), the solid lines show the calculated resonant wavelengths of the three-hole SCFs as functions of the core diameters, which agree well with the measured resonant dips of our samples.

In the processed PCF region, a portion of light power would propagate in the evanescent field, which provide a protected platform for light-matter interaction. The power ratio of evanescent field would, in general, increase with a higher ambient RI (smaller than the RI of waveguide) and a smaller core size. The dash lines in Fig. 7(a) are the calculated evanescent field of the fundamental mode with different ambient RIs (n_a) as functions of the core diameter, which indicate a significant increase of the ratio of evanescent field when n_a is close to the RI of waveguide material. The evanescent fields of the grating could be used in multiplex RI sensing by cascading the grating samples with different Bragg wavelengths. Material under test can be filled in the SCF region through micro-holes drilled on the outer jacket by using micro-machining techniques, such as fs laser drilling [12]. The RI sensitivity of the FBG-embedded PCF sensor is defined as $d\lambda_B/dn_a$ and can be calculated by the equivalent expression of $S_{RI} = 2\Lambda(\partial n_{eff}/\partial n_a)$ [13]. The lines in Fig. 7(b) show calculated RI sensitivity of grating embedded SCF regions as function of core diameter when n_a is 1.33 and 1.43. The sensitivity would increase with a similar trend as the evanescent field for the samples with smaller core and the test at higher n_a conditions.

Optics EXPRESS

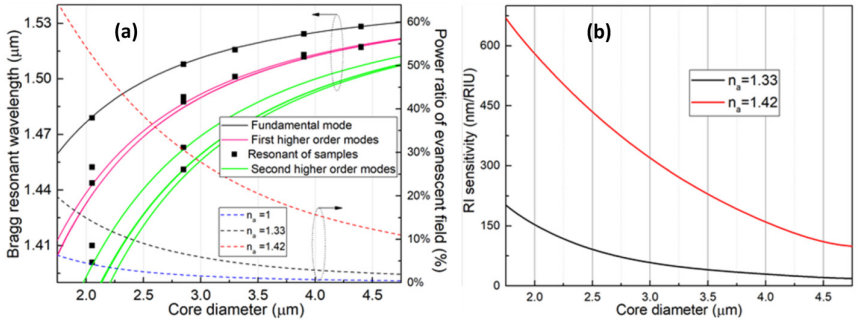

Fig. 7. (a) The calculated and measured Bragg resonant wavelength and power ratio of evanescent field of the three-hole SCF as functions of core diameter at the wavelength of 1550 nm. (b) The calculated RI sensitivity of the grating as functions of core diameter.

4. Sensing experiments

The FBG-embedded PCFs were tested to characterize their response to the changes of temperature, strain and liquid RI. The transmission and reflection spectra were measured by using a system constructed with a wideband laser, an optical circulator and an OSA.

For the test of static temperature response, a digitally controlled column oven (ECOM LCO-102) with 0.1 °C accuracy was used to provide a uniform temperature zone for the grating region. The red shift of the dip wavelength of a grating sample was ~0.92 nm in a test from 22.6 °C to 99.9 °C. The temperature sensitivity was ~11.9 pm/°C with good linearity, which is slightly higher than sensitivity of the FBGs on commercial SMF [2]. For the same sample, the sensitivity decreased to ~11.3 pm/°C when the in-fiber holey region was opened to the environment by drilling holes on the surface and struts of the SCF region. This could be explained by the release of the temperature induced tension during temperature raising.

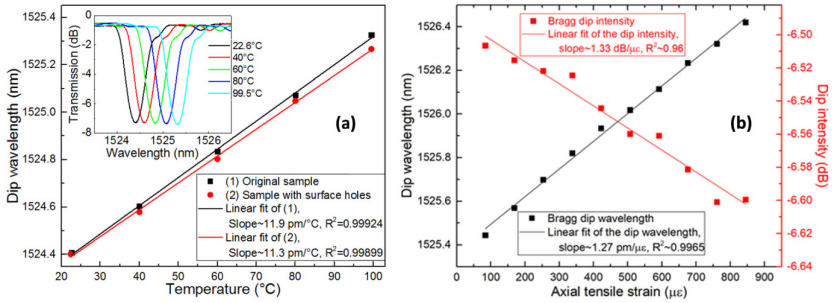

Fig. 8. (a) The response of sample-1 to the environmental temperature changes, inset: the transmission spectra of the sample-1 at different temperatures, (b) The spectral response of sample-2 to different axial tensile strains.

To test the static strain response, we used two fiber holders (561-FH from Newport Co.) to clamp both ends of a section of PCF grating sample. The fiber length between two holders was ~35 cm length. Then, one of the holder was fixed and the other was assembled on a translation stage, which was driven by micrometer with 10 μm resolution. Figure 8(b) shows the spectral response of a sample with core diameter of ~4.5 μm to axial tensile strains ranging from 80 με to 850 με. The slope of wavelength red shift during the test is ~1.27 pm/με, which is slightly larger than a SMF FBG and indicates no obvious stress concentration in the processed PCF region.

Another grating sample with core diameter of ~4.5 μm was used in the test of liquid RI response. The RI liquids from Gargille Co. with RI range from 1.37 - 1.436 was used in the experiment. The liquids were filled in the SCF region from the micro-holes drilled on the outer jacket of SCF region by fs laser [12]. To facilitate infiltration of the RI liquids, we cut the sample at a position close to the grating region. Figure 9 shows the reflection spectra of

Optics EXPRESS

the sample when different RI liquids are filled in the SCF region. After each measurement, the RI liquid in the holes was removed by ethanol and then the sample was dried at ~80 °C till the spectrum returned to the initial positon. The Bragg wavelength increased with the ambient RI nonlinearly as the inset of Fig. 9. The RI sensitivity of the sample is ~19 nm/RIU when the ambient RI is 1.33, and ~158 nm/RIU when the ambient index is 1.42, which agree well with the predicted values in last section. The RI sensitivity of grating embedded PCF would be enhanced by using samples with smaller core size.

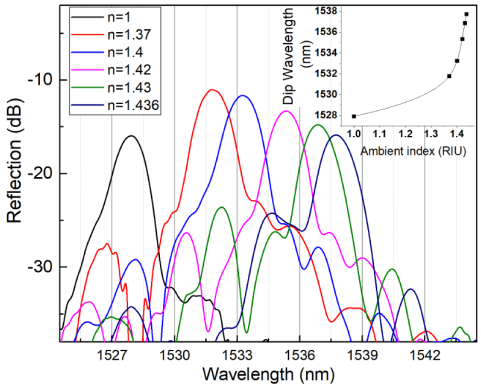

Fig. 9. The measured reflection spectra of sample-3 when the whole is filled with liquids with different RIs. Inset: the grating dip wavelength as function of ambient index.

5. Conclusion and prospect

In this work, we propose a method for efficiently fabricating Bragg grating in all-silica PCF. The key of the method is a selective inflation process before grating inscription. In the process, the periodic cladding structure of PCF can be locally transferred to a SCF structure with simpler cladding, which would be a "window" opened on the PCF for efficiently micro-machining from side direction of fiber, but also provide entrance for fluids infiltration to the core region of the PCF. In the local SCF regions on PCF, inscription laser would reach the fiber core with little loss when passing the outer jacket with typical thickness of 10 - 25 μm from side direction.

Bragg gratings were successfully built in the SCF regions with triangular-like core by use of a phase mask and a focused infrared fs laser with pulse energy as low as ~200 μJ. The SCF region with a smaller core size possesses a blue-shifted resonant wavelength, and exhibits a stronger grating resonance with a shorter exposure time under the same fabrication condition. A grating with ~99.75% reflectivity was realized in a sample with core diameter of ~2 μm. The Bragg and higher order mode resonances of the gratings in SCF regions are verified based on the numerical simulations.

The static temperature and strain responses of the grating resonant dips are respectively 11.3 pm/°C and 1.3 pm/με for the samples with core diameter of ~4.5 μm, which are comparable to the sensitivities of the FBGs on commercial SMF. However, the grating in the pure silica SCF region could sustainable at high temperature [14], and it would response to the RI variance in the evanescent-field region. Compare to the Bragg gratings inscribed on micro-/nano-fibers, these gratings are robust and resistant to environmental contaminations.

This grating inscription technique is useful in building various grating-integrated PCF devices, and could also be applied on some other holey fibers for efficient grating inscription. To the PCF, the technique is flexible in making gratings with different properties on the SCF regions with different internal structures, which can be realized by selectively inflating different air-columns in fiber [10]. For example, the gratings inscribed in the SCF regions with highly birefringent core would have two Bragg resonant peaks in spectrum which could be useful in two-parameter sensing.

The functionality of the grating embedded PCFs could be further enhanced by introducing new structures or materials into the SCF regions, which are convenient for

Optics EXPRESS

lateral micromachining and fluid infiltration. For example, micro-cantilever can be made based on the grating-embedded core [15]. The structure could be used for multi-point acceleration measurement. In addition, the tailorable evanescent field of the grating would enable a range of light-matter-interaction-based applications. Besides the RI sensing introduced in this article, this PCF grating could be used to build micro-fluidic laser by infiltrating laser dye into the grating region and pumping the dye with lateral incident or in-fiber light.

Fundings

National Natural Science Foundation of China (NSFC) (61405125, 61425007, 61505120 and 61635007); China Postdoctoral Science Foundation (2015M572351 and 2016T90796); Guangdong Natural Science Foundation (2014B050504010, 2015B010105007, 2015A030313541, and 2014A030308007); Science and Technology Innovation Commission of Shenzhen (grant nos. JCYJ20150324141711614, JCYJ20160427104925452, and JCYJ20160307143501276).